Photon Pair Production in Coupled Lithium Niobate Nanowaveguides

Samuel M. B. Winter

Department of Physics, University of Bath, Bath BA2 7AY, United Kingdom

E-mail: sc210@bath.ac.uk

Abstract. This work aims to design a device for photon pair generation with a pair of parallel lithium niobate on insulator (LNOI) straight waveguides. The device uses a pulsed laser operating in the telecommunications bands at 1.504 μm to produce non-degenerate photon pairs with wavelengths of 1.41 μm and 1.61 μm. The device uses second harmonic generation and spontaneous parametric down conversion to convert the wavelengths of the photons. The field envelope functions and their evolution down the length of the waveguides were simulated and the joint spectrum of the two photon state was calculated from these results, yielding a purity of $\mathcal{P} = 16.7\%$.

Introduction

Photonic quantum technologies are of great interest as they offer increased security of communications in the case of quantum key distribution [1]. New computing technology is the case of quantum computing that would allow for much more intensive quantum simulation and other mathematical problems such as optimisation [2] and also neuromorphic computing and other quantum artificial intelligence [3]. All of these technologies have a key roadblock preventing the scalability of the devices, that is the production of single photons with the required properties, namely being in a pure quantum state [4–6]. Quantum key distribution has less stringent requirements on the purity of the photon states produced, however it is still limited by the rates of the photon production [7].

Lithium niobate (LN) photonics have been shown to be a promising candidate, due to its high $\chi^{(2)}$ non-linearity ($d_{33} = 27$ pmV^{-1}) [8]. LN is also transparent over most of the infrared and visible spectrum, and a broadband region of operation for second harmonic generation (SHG) and spontaneous parametric down conversion (SPDC) processes [9]. SPDC promises much higher photon generation rates than spontaneous four wave mixing (SFWM) in silicon. SFWM yields much lower photon generation rates however due to the magnitude of the the $\chi^{(3)}$ non-linear coefficient of silicon, ally more desirable than those generated through SPDC [10; 11]. The intrinsic energy and momentum conservation laws in SPDC typically have anti-correlated spectra that are less desirable, as they provide distinguishing information and produces a mixed quantum

state of the photon pair. This can be combatted by tight filtering - although this reduces the photon generation rate, or by changing the geometry of the devices to control the dispersion properties of the waveguide.

Previous research indicates the potential to increase the purity of the two photon state of the device to higher purities, and with high photon generation rates. Work on single waveguides with periodic poling to achieve quasi-phasematching has reached purities of 88% [12], in separate modes with a short wavelength pump laser. This theoretical work produced degenerate photon pairs at 1550 nm, that cannot be split by WDM. This may be solved by changing the wavelength of the pump laser so that a pair of non-degenerate photons may be produced with polarisation entanglement that can still be separated with WDM. Work into LN waveguides suspended in a cladding material has seen promising results [13], with high photon pair generation rates of the order of 5 MHz, but they are still strongly anti-correlated and thus have low purity. High rates of single photons in a single waveguide of periodically poled LN have been observed with rates of 11 MHz, and high purities, greater than 71% [14].

In this work we propose the design of a pair of nano scale waveguides that will take advantage of the SHG and SPDC processes to produce photon pairs from a pulsed laser operating in the telecommunications band. The device will generate photons at wavelengths above and below the pump laser, allowing for a lot of noise to be filtered out.

1. Device Design

1.1. Waveguide 2 Geometry

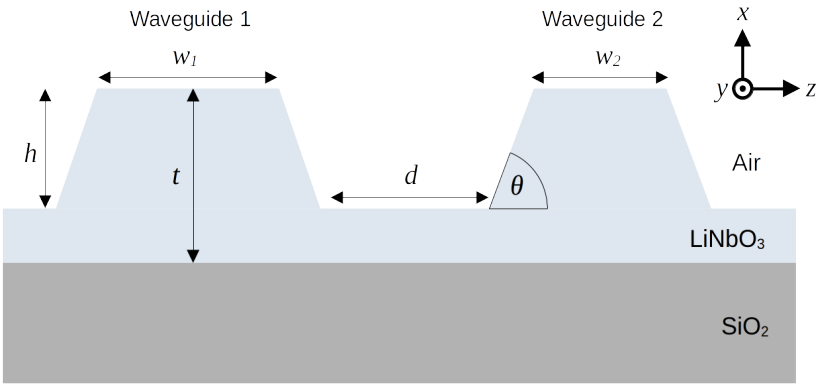

Figure 1. The cross-sectional view of the waveguides where w_1 and w_2 are the waveguides' widths, h is the waveguides' height, d is their separation, and θ is the sidewall angle. Note that each waveguide must have the same height due to the manufacturing process. The cross sectional geometry is constant down the waveguides' length and forms a pair of straight waveguides. The waveguides in this model are directly exposed to air.

A cross-sectional view of the device can be seen in figure 1. The device will take a laser pulse into waveguide 1 at a fundamental frequency ω_f, in the fundamental TE mode. The non-linear properties of LN will allow for the generation of second harmonic photons in waveguide 1 at a frequency $2\omega_f$. The geometry will have optimal coupling between the two waveguides for the higher order modes so that the higher frequency photons will couple across to waveguide 2, while the fundamental mode will not couple due to the differences in the waveguides' widths. Finally, the photons in waveguide 2 will split up through SPDC and can be observed at the other end of the device in waveguide 2. The laser pulse used for this device was modelled as a Gaussian pulse with a width (defined as 2 standard deviations) of $t_0 = 7$ ps.

The structure can be manufactured through standard etching techniques and chemomechanical polishing to create a low loss, precise, nano scale waveguide [15; 16]. The low loss is due to the reduced surface roughness with this manufacturing technique. The model has a thin layer of LN to model the residual LN from the manufacturing process, for the same reason there is a sidewall angle that creates the trapezoidal shape as right angled waveguides would be much more challenging to etch. The geometry parameters that have given the best results were $t = 350$ nm, $h = 330$ nm, $w_1 = 664$ nm, $w_2 = 500$ nm and $\theta = 70°$. The separation was set to $d = 430$ nm as this gave a long enough coupling length for a single coupling exchange to happen over the length of the waveguide, that is $L = 9800$ μm.

To choose the geometry, each waveguide was modelled in isolation first. The wavelength of photon pairs produce in waveguide 2 are dictated by its cross section geometry. The final quantum state can be described by $|\psi\rangle = |0\rangle + \gamma|\psi_2\rangle$ where γ is small in magnitude [17]. The $|0\rangle$ ket describes the vacuum state and the $|\psi_2\rangle$ ket describes the two photon state. The approximation of small γ comes from assumption that the pump is non-depleting, as SPDC is a very inefficient process. The photon state is given by [18]

$$|\psi_2\rangle = \iint \mathcal{J}|\omega_s\rangle|\omega_i\rangle d\omega_s d\omega_i \tag{1}$$

where $|\omega_s\rangle$ and $|\omega_i\rangle$ are the single particle Fock states at the frequency of the signal and idler photons respectively. $\mathcal{J}$ is the joint spectral amplitude, which can be approximated at the product of a phasematching function Φ and the pump field spectrum $\widetilde{U}_p$. Φ captures the momentum conservation law and shows which pairs of photons can be produced by the corresponding pump wavelength $\omega_p = \omega_s + \omega_i$. $\widetilde{U}_p$ describes the amplitude of each pump frequency present in the device. To calculate which wavelengths will be produced, the spectrum is assumed to have the Gaussian form $\widetilde{U}_p = \exp(-(\omega_0 - \omega_i - \omega_s)^2/\Delta\omega^2)$, with $\omega_0 = 0.752$ μm as the central frequency. This is plotted in wavelength space as $= 2\pi c/\omega$. Under these assumptions, the phasematching function is reduced to

$$\Phi = \text{sinc}\left(\frac{L\Delta\beta}{2}\right) \tag{2}$$

where L is the length of the waveguide and $\Delta\beta = \beta_p - \beta_i - \beta_s$ is the difference in the propagation constants of the pump, idler and signal photons. COMSOL was used to find the effective refractive indices and hence $\beta = 2\pi n_{eff}/\lambda$ where lambda is the free space wavelength. The phasematching function for the selected geometry of waveguide 2 ($w_2 = 500$ nm) is shown in figure 2 where the black dashed line indicated the central wavelength of $\widetilde{U}_p$, this is set to $_0 = 0.752$ μm.This selection of pump laser and geometry came from plotting the phasematching function for several top widths, and finding maxima of Φ at useful pairs of wavelengths, typically in the O and C or L telecommunications bands, when pumped by a ~ 0.775 μm laser. The pump function $\widetilde{U}_p$ must intersect two separate regions of the phasematching curve to get distinct wavelengths which then allows the two photons to be separated by wavelength division multiplexing. The refractive index of the pump photon mode was found to be $n_p = 1.5269$.

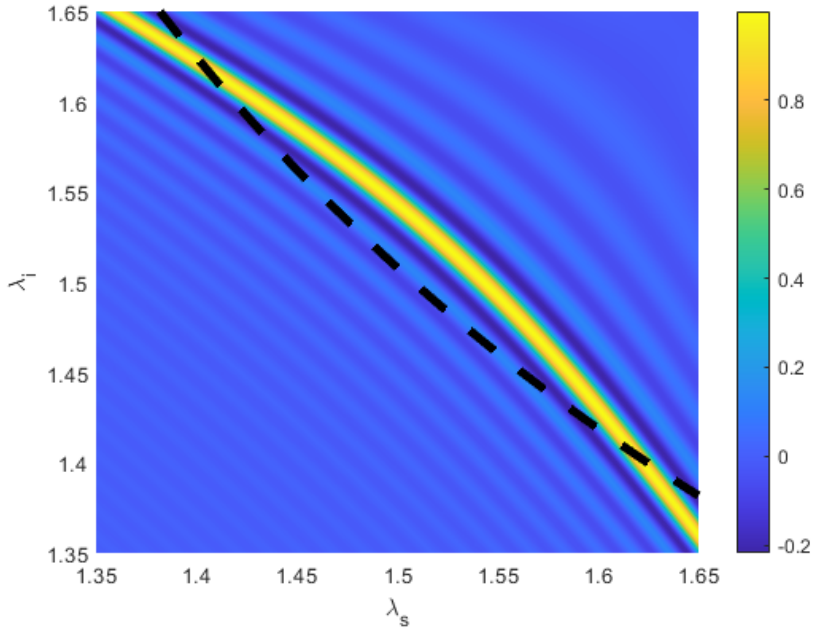

Figure 2. The phasematching function of a single waveguide geometry. The yellow maximum shows the perfectly phasematched pairs of wavelengths. The black dashed line indicates the central wavelength of the pump function $\widetilde{U}_p$. Where these two bands intersect will be the maxima of the joint spectrum, and indicate the pairs of wavelengths that could be produced.

1.2. Waveguide 1 geometry

The SPDC process will be driven by photons coupling from waveguide 1 into waveguide 2. In order to couple optimally, the refractive indices of the mode populated by the 0.752 μm photons must have the same refractive index, but the top widths of the waveguides must be different in order to prevent coupling in the other modes as they would all have

the same refractive index. Figure 3 shows the refractive index of several modes in the isolated waveguide 1 modes as a function of width. The crossing points with the black dotted line show the widths at which there is a mode with the required refractive index. Of the four crossing points, only $w_1 = 664$ nm is suitable. The crossing at 500nm can be written off as w_1 can be the same as w_2. With a top width of 338 nm, there is no guided mode for the laser input pulse at 1.504 μm, so would be unsuitable. The mode that crosses at 553 nm is a TM mode and the difference in the polarisation states of the modes prevents strong coupling. SHG is a much more efficient process than SPDC, so the device is optimised for the latter process. There will be a large loss in input power, however there is efficient coupling so there is little loss in power from the SHG photons through coupling.

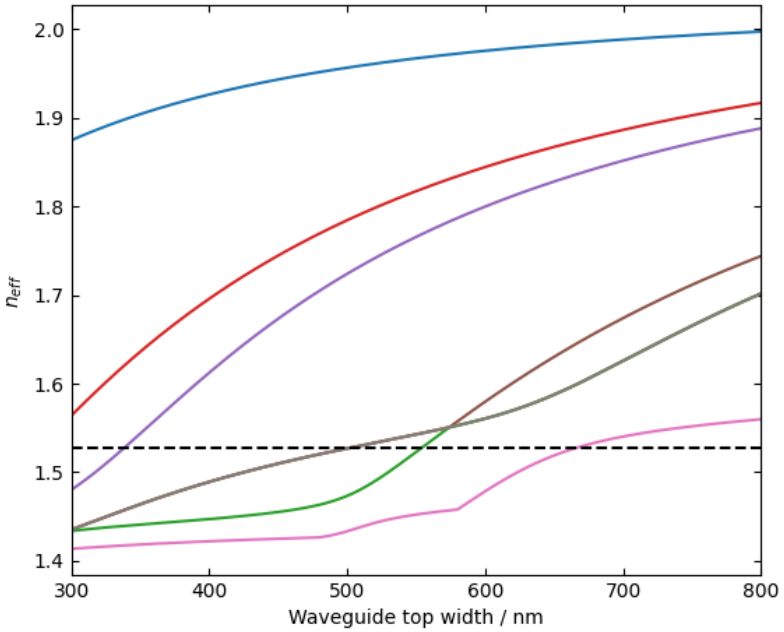

Figure 3. The plot of refractive index against width. Some series overlap onto each other as the COMSOL solver converged onto the same series when changing the width. Of the three crossing points, the 500 nm top width is unsuitable as the waveguides cannot be identical as all modes would then couple. In the shorter waveguide crossing at 338 nm, the fundamental mode that would be pumped with the laser pulse is not guided, making it unusable. Therefore only the longer waveguide top width of 664 nm can be used.

1.3. Characterising the Coupling Process

In the dual waveguide geometry it is important to know the coupling strength as this dictates the length of the waveguide pair. The coupling constant $C = (\beta_+ - \beta_-)/2$ where β_+ and β_- are the propagation constants in the supermodes formed by the coupling.

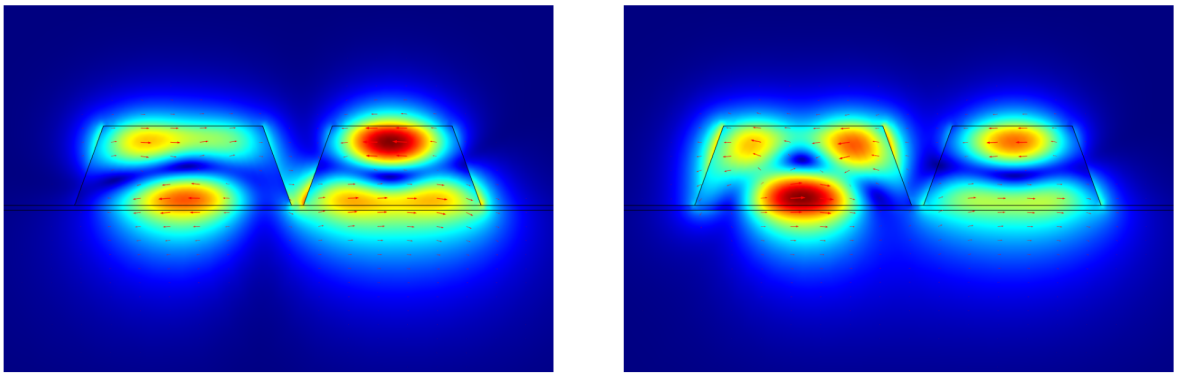

Figure 4. The coupling of the phasematched modes can be seen here with the arrows indicating the polarisation states. The effective refractive indices at a wavelength of 0.753 μm are 1.5289 for the mode on the left and 1.5257 for the mode on the right. These lie above and below $n_p = 1.5269$ respectively.

These are slightly higher and lower than n_p in the isolated waveguides as predict. The coupling constants were calculated as a function of separation and ed by perturbation theory. The results can be seen in figure 5. An exponential curve was fitted to the data using the SciPy Python library to extrapolate the coupling to larger separations where COMSOL fails to find the coupled modes.

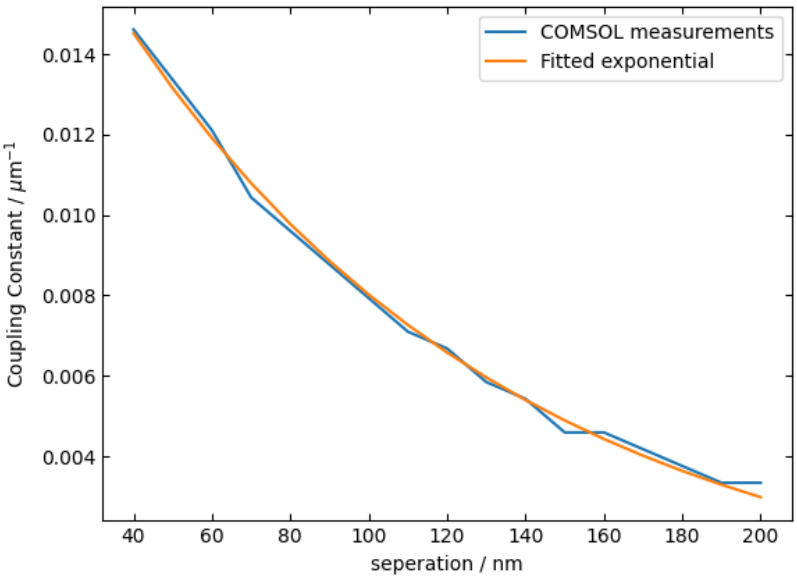

Figure 5. The coupling constant decays exponentially as a function of separation. The COMSOL simulations yield a decaying function as expected. The smooth fitted curve is used to extrapolate for separations too large for COMSOL to find the coupled modes, such as those used in the scale of the final device.

Modelling the Pump Field

Firstly, the propagation constants β_m and their jth derivatives, with respect to angular frequency ω, β_{mj}, were found for the chosen geometry parameters using COMSOL. Here, $m \in \{f, s, p\}$ denotes the chosen mode for the fundamental mode that is excited using the telecommunications laser in waveguide 1, the mode chosen for the second harmonic in waveguide 1, and the mode that will pump the SPDC process in waveguide 2. The free space wavelengths of photons in each mode are $\lambda_f = 1.504$ μm and $\lambda_s = \lambda_p = 0.752$ μm. The propagation of each mode down the length of the waveguide is modelled using a normalised field envelope function U_m. To solve the equations numerically, the field amplitudes and coordinates are normalised and set into the reference frame of the fundamental mode pulse. The normalised distance coordinate $\xi = y/y_d$, where $y_d = 2t_0^2/|\beta_{f2}|$ is the dispersion length. The normalised time coordinate $\tau = (t - y\beta_f)/t_0$ is set such that the centre of the pulse in the fundamental mode always has $\tau = 0$. The fields are scaled as $U_f = \sqrt{2}\rho_2 y_d A_f$ and $U_{s,p} = \rho_2 y_d A_{s,p}$ such that $|A_m|^2$ yields the intensity in watts. ρ_2 is the effective non-linear coefficient. The evolution of all 3 fields is described by [19–21]

$$\begin{cases} i\partial_\xi U_f = -r_2\partial_\tau^2 U_f - U_s U_f^* e^{i\kappa\xi} \\ i\partial_\xi U_s = -s_1\partial_\tau U_s - s_2\partial_\tau^2 U_s - \dfrac{U_f^2}{2} e^{-i\kappa\xi} + gU_p \\ i\partial_\xi U_p = -p_1\partial_\tau U_p - p_2\partial_\tau^2 U_p + gU_s \end{cases} \tag{3}$$

where $r_2 = -\beta_{f2}/|\beta_{f2}|$, $s_2 = -\beta_{s2}/|\beta_{f2}|$, $p_2 = -\beta_{p2}/|\beta_{f2}|$, and $s_1 = y_d/y_{ws}$, $p_1 = y_d/y_{wp}$. $y_{wm} = t_0/(\beta_m - \beta_f)$ is the walk-off length, noting that $y_{wf} = 0$. The normalised phasematching parameter $\kappa = -y_d\Delta\beta = -y_d(2\beta_f - \beta_s)$. SHG is most efficient when $\Delta\beta = 0$ as momentum is fully conserved in that interaction. The coupling constant $g = y_d C$ is the normalised coupling constant. In order to solve the coupled field equations 3, the Fourier transform is taken in the τ domain. The Fourier transform used is defined in terms of normal frequency, $\mathscr{F}(f(\tau)) = \int_{-\infty}^{\infty} f \exp(-2\pi i\nu\tau)\, d\tau = \tilde{f}(\nu)$, so that the ∂_τ operators become $2\pi i\nu$ terms, creating coupled ODEs in ν space. A 4th order Runge-Kutta solver, implemented in Python, was used to numerically solve the equations. A Gaussian pulse was used at the initial condition for U_f with a peak amplitude of 1, the other fields have zero amplitude initially. The results of this simulation can be seen in figure 6.

There is a much faster exchange of photons between the f and s modes, which can be seen in figure 6 (b). These fast exchanges are due to the phase mismatch κ being large for this geometry so the typical interaction length for this process is very small. The coupling length is set to be the approximate length of the waveguide to yield a single 'pulse' in waveguide 2. The separation was set to $d = 430$ nm and the length of the device is $L = 9800$ μm. When there are both coupling and SHG processes impacting $\widetilde{U}_s$, a bifurcation appears in the centre of the waveguide, in the spectrum.

When t_0 is decreased, the bandwidth of the pulse's spectrum is increased. At

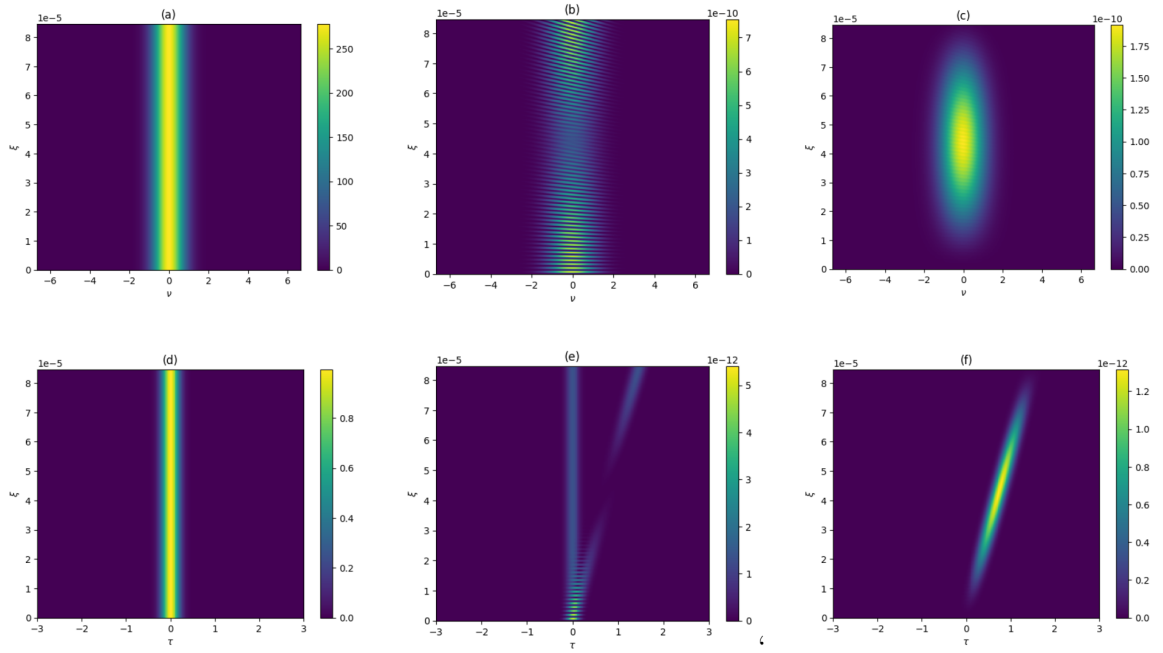

Figure 6. The spectra and pulse intensity as a function going down the waveguide. The angles in (e) and (f) come from the difference in the group velocities in the s and p modes. The spectra (a-c) show the very fast exchange in energy of U_f and U_s in the SHG process. The presence of a single peak in (c) comes from adjusting the coupling length until it reached approximately 9800 μm. The length of waveguides simulated here are 9800 μm.

frequencies further from the centre, it appears that they oscillate in amplitude faster, hence the pointed shape in figure 7. The areas of increased intensity at either side of the top of the pulse have alternate phases to the initial pulse.

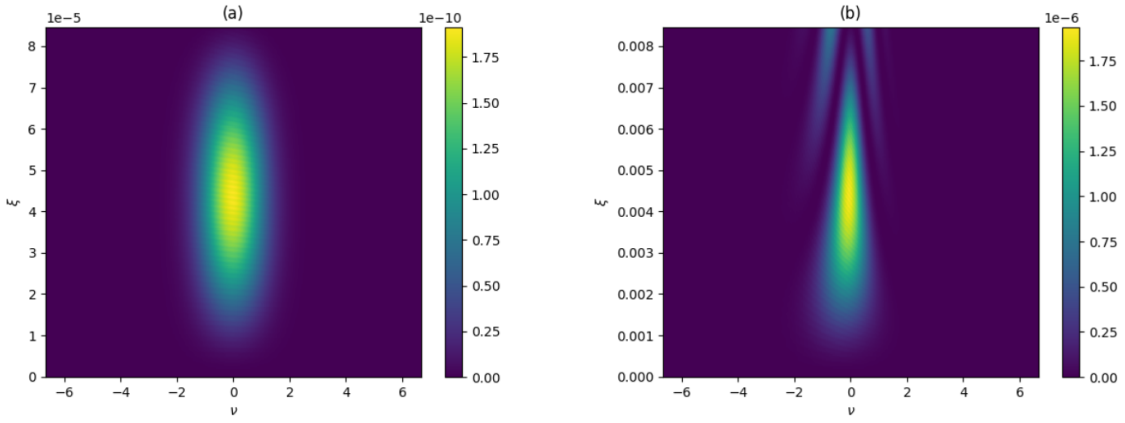

Figure 7. In each of the spectra fine ridges can be observed due to the peaks in amplitude in $\widetilde{U}_s$. (a) shows the spectrum with $t_0 = 7$ ps and has a rounded isolated pulse. (b) show the spectrum with $t_0 = 0.7$ and has 'wings' from the faster oscillations of frequencies further from the centre. The width of the spectrum is much broader due the bandwidth being inversely proportional to t_0.

Joint Spectrum

The geometry of waveguide 2 is optimised for the SPDC process from the mode that U_p is in into the fundamental TE mode. With the specified geometry parameters figure 8 shows the joint spectral intensity of the produced photons. A key parameter of the system is the initial pulse width t_0. If the pulse width is too small, the spectrum becomes broader. Frequencies further away from the central frequency oscillate faster in ξ, so when the integral to calculate $\mathcal{J}$ is evaluated there is cancellation from the change of sign from each oscillation. Therefore the pulse width must be broad enough to keep all of the frequencies close enough together to maintain the structure of the joint spectral intensity. The effect on $\widetilde{U}_p$ can be seen in figure 7. The other key parameter is the length of the waveguide pair. The phasematching function becomes narrower as L is increased. This effect approximately reduces the height of the $|\mathcal{J}|^2$ streaks on the graph, while t_0 affects the width.

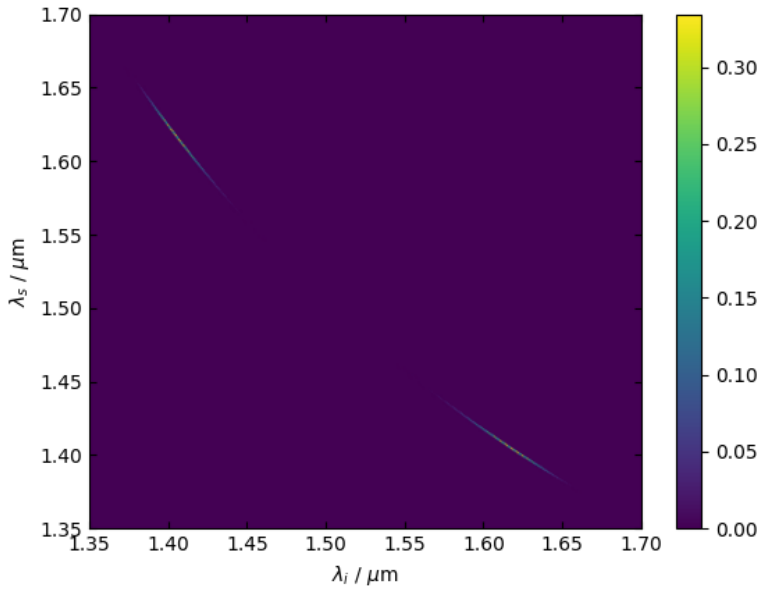

Figure 8. The joint spectral intensity, $\mathcal{J}$, of the final device.

In order to prevent interference there must be a single peak in the power of the U_p field, which is controlled by the coupling between the two waveguides. The waveguide length and coupling length were adjusted until the phasematching curve was fine enough, then the pulse width adjusted to remove the wings and interference seen in $\widetilde{U}_p$. When t_0 is too small, the interference in $\widetilde{U}_p$ forces $|\mathcal{J}|^2$ to become very narrow yielding almost no amplitude or visible peaks in the joint spectrum. The aim of these adjustments was to attempt to increase the purity of the two photon state produced. Balancing these two effects landed on the final geometry of the device.

Photon Purity

Photon purity described how many states the photons are in a superposition of. If the purity is high, the photons are highly indistinguishable and therefore behave in the way required for photonic quantum computing. The Schmidt decomposition of $\mathcal{J}$ yields the coefficients b_k, required for calculating the purity, in the expansion of the quantum state

$$|\psi\rangle = \sum_k b_k \phi_k(\omega_i)\phi_k(\omega_s) \tag{4}$$

where ϕ are the Schmidt functions [22]. The series b_k can be used to find the photon purity

$$\mathcal{P} = \frac{\sum_k b_k^2}{\left(\sum_k b_k\right)^2}. \tag{5}$$

Applying this to the $\mathcal{J}$ yields a final photon purity of $\mathcal{P} = 16.7\%$. The photons produced by this device are not yet suitable for quantum computing, where purities must be upwards of 98% however, they are suitable for quantum key distribution as this is not a requirement for this technology.

General Discussion

Periodic poling is a common technique used in these devices to more easily match the phasematching conditions however, we have tried to avoid using it in this device. The length scales required for periodic poling in LN are typically very small so this is hard to achieve consistently. Furthermore, the process is not permanent (although the device lifetime is still high). One of the main reasons it was not simulated in this work is that periodic poling requires an extra manufacturing step that would increase the cost of production and the reproducibility, especially of an array of these devices.

Future simulations using this model should aim to increase the purity of the produced photons, and to calculate the conversion efficiency. There are several techniques that could be employed to increase the purity of the photons, including producing them in different modes. This would change the geometry of the phasematching function and allow for more control of the shape of the joint spectral intensity. Work into tuning the output photons wavelengths to be closer is also desirable, especially if higher purity can be achieved.

Conclusion

In this work we have developed a model for a pair of coupled nano scale waveguides. The device leverages the high χ^2 non-linearity of LN for SHG and SPDC processes to take a telecommunications laser, and generate photons at two new wavelengths. The joint spectrum of the two photon state this device produces, shows the pairs of photons possible, and multiple geometry parameters have been discussed along with their effect

on the joint spectrum. A final photon purity was calculated as $\mathcal{P} = 16.7\%$. Future work into simulating different combinations of modes, and possibly periodically poling the waveguides has been suggested.

Acknowledgments

I would like to thank my project partner for his support throughout the project and in modelling and generating the data. I would also like to thank my supervisors, Dr. Peter Mosley and Dr. Andriy Gorbach for their help and direction.

References

[1] Mao Y, Zeng P and Chen T Y 2021 *Advanced Quantum Technologies* **4** 2000084 ISSN 2511-9044

[2] Moussa C, Calandra H and Dunjko V 2020 *Quantum Science and Technology* **5** 044009 ISSN 2058-9565

[3] Shastri B J, Tait A N, Ferreira de Lima T, Pernice W H P, Bhaskaran H, Wright C D and Prucnal P R 2021 *Nature Photonics* **15** 102–114 ISSN 1749-4893

[4] Devitt S J, Stephens A M, Munro W J and Nemoto K 2011 *New Journal of Physics* **13** 095001 ISSN 1367-2630

[5] Kitaev A Y 1997 *Russian Mathematical Surveys* **52** 1191–1249

[6] Kok P, Munro W J, Nemoto K, Ralph T C, Dowling J P and Milburn G J 2007 *Reviews of Modern Physics* **79** 135–174

[7] Diamanti E, Lo H K, Qi B and Yuan Z 2016 *npj Quantum Information* **2** 1–12 ISSN 2056-6387

[8] Xue D, Betzler K and Hesse H 2001 *Journal of Applied Physics* **89** 849–854 ISSN 0021-8979

[9] Yuan S, Hu C, Pan A, Ding Y, Wang X, Qu Z, Wei J, Liu Y, Zeng C and Xia J 2021 *Journal of Semiconductors* **42** 041304 ISSN 1674-4926

[10] Spring J B, Mennea P L, Metcalf B J, Humphreys P C, Gates J C, Rogers H L, Söller C, Smith B J, Kolthammer W S, Smith P G R and Walmsley I A 2017 *Optica* **4** 90

[11] Silverstone J W, Bonneau D, Ohira K, Suzuki N, Yoshida H, Iizuka N, Ezaki M, Natarajan C M, Tanner M G, Hadfield R H, Zwiller V, Marshall G D, Rarity J G, O'Brien J L and Thompson M G 2014 *Nature Photonics* **8** 104–108 ISSN 1749-4885, 1749-4893

[12] Ebers L, Ferreri A, Hammer M, Albert M, Meier C, Förstner J and Sharapova P R 2021 *arXiv:2110.10562 [physics, physics:quant-ph]*

[13] Chen J y, Meng Sua Y, Ma Z h, Tang C, Li Z and Huang Y p 2019 *OSA Continuum* **2** 2914

[14] Zhao J, Ma C, Rüsing M and Mookherjea S 2020 *Physical Review Letters* **124** 163603

[15] Wang M, Wu R, Lin J, Zhang J, Fang Z, Chai Z and Cheng Y 2019 *Quantum Engineering* **1** e9 ISSN 2577-0470

[16] Lin J, Zhou J, Wu R, Wang M, Fang Z, Chu W, Zhang J, Qiao L and Cheng Y 2019 *Micromachines* **10** 612 ISSN 2072-666X

[17] Main P, Mosley P J, Ding W, Zhang L and Gorbach A V 2016 *Physical Review A* **94** 063844

[18] Grice W P and Walmsley I A 1997 *Physical Review A* **56** 1627–1634

[19] Rowe W R, Skryabin D V and Gorbach A V 2019 *Physical Review Research* **1** 033146

[20] Taylor H and Yariv A 1974 *Proceedings of the IEEE* **62** 1044–1060 ISSN 1558-2256

[21] Gorbach A V and Ding W 2015 *Photonics* **2** 946–956 ISSN 2304-6732

[22] Eberly J H 2006 *Laser Physics* **16** 921–926